Biogeosciences
Discussions

Diurnal versus spatial variability of greenhouse gas emissions from an anthropogenic modified German lowland river

Matthias Koschorreck[1], Norbert Kamjunke[2], Uta Koedel[3], Michael Rode[4], Claudia Schuetze[3], Ingeborg Bussmann[5]

5 [1]Department Lake Research, Helmholtz Centre for Environmental Research, Magdeburg, Germany
[2]Department River Ecology, Helmholtz Centre for Environmental Research, Magdeburg, Germany
[3]Department Monitoring & Exploration Technologies, Helmholtz Centre for Environmental Research, Leipzig, Germany
[4]Department Aquatic Ecosystem Analysis, Helmholtz Centre for Environmental Research, Magdeburg, Germany
[5]Department Shelf Sea System Ecology, Alfred Wegener Institut, Helmholtz Zentrum für Polar- und Meeresforschung,
10 Helgoland, Germany

Correspondence to: Matthias Koschorreck (matthias.koschorreck@ufz.de)

Abstract.

Greenhous gas (GHG) emissions from rivers are globally relevant, but quantification of these emissions comes with considerable uncertainty. Most of the existing studies were carried out at small streams and much less is known about GHG

15 emissions from larger rivers. Here quantification of ecosystem scale emissions is challenged by both spatial and short-term temporal variability. We measured spatio-temporal variability of CO_2 and CH_4 emissions from a 1 km long reach of the German lowland river Elbe over three days in order to establish which factor is more relevant to be taken into consideration: small-scale spatial variability or short-term temporal variability of CO_2 and CH_4 emissions.

GHG emissions from the river reach studied were dominated by CO_2 and 90 % of total emissions was from the water surface,

20 while 10% of emissions was from dry fallen sediment at the side of the river. Aquatic CO_2 emissions were similar at different habitats, while aquatic CH_4 emissions were higher at the side of the river. Artificial structures to imoprove navigability (groynes) created still water areas with elevated CH_4 emissions and lower CO_2 emissions. CO_2 emissions exhibited a clear diurnal pattern, but the exact shape and timing of this pattern differed between habitats. In contrast, CH_4 emissions did not change diurnally. Our data confirm our hypothesis that spatial variability is important for CH_4 while diurnal variability is more

25 relevant for CO_2 emissions. Continuous measurements are most likely necessary for reliable quantification of river GHG emissions.

1 Introduction

1.1 Necessity of upscaling/quantification of GHG emissions from rivers

Rivers are a globally relevant source of greenhouse gases (GHG) (Battin et al., 2023; Attermeyer et al., 2021; Raymond et al.,

30 2012). It is currently estimated that rivers globally emit about 2 Pt CO_2 y^{-1} (Liu et al., 2022) and 30.5 ± 17.1Tg CH_4 y^{-1}

(Rosentreter et al., 2021). However, these estimates suffer from considerable uncertainty. Aquatic GHG emissions actually generate considerable uncertainty among global GHG assessments (IPCC, 2021). Reducing uncertainty in aquatic GHG budgets is important in order to improve biogeochemical models and climate prediction(s). Uncertainties result from a general lack of data as well as from the methods used for budgeting aquatic GHG emissions.

1.2 Traditional method for budgeting

Bottom-up approaches to quantifying riverine GHG emissions are typically based on GHG concentrations measured in a restricted number of water samples. GHG fluxes between water and atmosphere are calculated from measured concentrations and estimated gas transfer velocities (Raymond et al., 2013) multiplied by water surface area. Typical datasets contain weekly to monthly concentration data from a small number of sites along a specific river. GHG emissions can also directly be measured by floating chambers. However, these measurements are laborious and prone to experimental artefacts if not carried out carefully (Lorke et al., 2015). Water surface areas are typically estimated by using river width based on empirical relations (Raymond et al., 2013) or for larger rivers using remote sensing data (Palmer and Ruhi, 2018). These approaches are suitable to cover seasonal dynamics as well as large-scale spatial patterns along larger rivers. However, recent research has indicated considerable short-term temporal and small-scale spatial variability of riverine GHG emissions which pose challenges for budgeting and upscaling.

1.3 Short-term temporal variability

The advent of reliable and affordable probes to continuously measure GHG concentrations revealed considerable diurnal fluctuations of CO_2 in rivers (Gómez-Gener et al., 2021). Because the balance between photosynthesis and respiration depends on light, CO_2 emissions are typically elevated in the night (Attermeyer et al., 2021). Thus, CO_2 emission estimates only relying on discrete water samples taken during daylight hours significantly under-estimate true emissions. While diurnal fluctuations of CO_2 are well documented, there is little knowledge concerning the short-term variability of CH_4 (Stanley et al., 2016).

1.4 Small scale spatial variability

While a single water sample might be representative of a certain specific reach in a small stream this is undoubtedly not the case in larger rivers. Rivers contain various habitat types: these are either natural or those or with anthropogenic modifications. Channelisation and disconnection of rivers from their floodplain decrease spatial heterogeneity (Wohl and Iskin, 2019) and most likely also affect GHG emissions (Machado dos Santos Pinto et al., 2020). However, anthropogenic modifications not only reduce habitat diversity. Several European rivers were modified by building groynes in the 19th century with the primary goal of concentrating the water into the main river and to improve river flow and navigability (Pusch and Fischer, 2006). Consequently, the flow velocity is lower within the groyne fields leading to increased sedimentation (Kleinwächter et al., 2017). Thus, groynes increase habitat diversity compared to straight, channelised rivers but decrease it compared to a natural

shoreline. In the River Elbe, there are no groynes until German river km 120; however, they dominate the shore line downstream from there (Fig. 1b). A recent study presents evidence that the still water areas between such groynes are a source of CH_4 resulting in lateral CH_4 gradients (Bussmann et al., 2022). Ignoring these gradients significantly under-estimates total CH_4 emissions.

65   A typical feature of rivers is their fluctuating discharge resulting in fluctuating water level. Thus, depending on discharge, certain parts of rivers are temporarily drying up. It has been shown that these dry river areas emit disproportionally high amounts of CO_2 into the atmosphere (Gómez-Gener et al., 2015). Ignoring dry areas in river GHG budgets may lead to a significant underestimation of GHG emissions (Marcé et al., 2019). Depending on their elevation, such dry river sediments can be quite heterogeneous with respect either to substrate type (sand versus mud), or to the occurrence of temporary vegetation
70   (Bolpagni et al., 2019). Recent research indicates considerable spatial variability as well as temporal dynamics of dry river GHG emissions (Mallast et al., 2020; Koschorreck et al., 2022).

1.5 Aim of this study

We expected that small-scale spatial and diurnal variability would need to be considered for budgeting GHG emissions from rivers. The ideal approach would thus be to perform high-frequency measurements at a large number of sites. However, this is
75   simply not possible and thus, there is a trade-off between frequency and spatial coverage of measurements. In this study, we aim to answer the question "What is more important for budgeting/upscaling GHG emissions from rivers: small-scale spatial or short-term temporal variability?". We hypothesise that the answer to this question depends on the gas: We expected spatial heterogeneity to be more relevant for CH_4 emissions, while temporal variability is more relevant for CO_2. To test this hypothesis, we measured CH_4 and CO_2 emissions in different habitats within a typical reach of the German lowland river Elbe
80   over a four-day campaign. The study was designed to cover a typical low-discharge summer situation when both habitat diversity and biological activity in the river were expected to be the highest.

2 Materials and Methods

2.1 Study Site

Investigations were performed at an one km-long reach of the 8th order River Elbe at Tangermünde located in the middle part
85   of the river in Germany at river km 388 according to German kilometration (Figure 1a). The reach is typical for the middle Elbe River which is characterised by groyne fields (Figure 1b) between km 120-580. Measurements were done in late summer on 18-22 August 2022. Discharge varied between 189-197 m^3 s^{-1} during that period which was below the mean low discharge of 235 m^3 s^{-1} (Figure 2).

We separated the river's water surface into three distinct habitats: The middle of the river, the sides of the river, and the area
90   between groynes (groyne fields). The groyne fields extend from the riverbank to a virtual line connecting the heads of the

groynes. The side areas we defined as extending from the outer boundary of the groyne fields 15 m into the river. The studied reach had ten groynes at both banks, extending up to 60 m into the river. The distance between the groynes was 80 ± 10 m. The area between the groynes was partly dry. These dry areas featured three typical habitats: muddy areas and sandy beaches without and with terrestrial vegetation (Figure 1c, Figure S1).
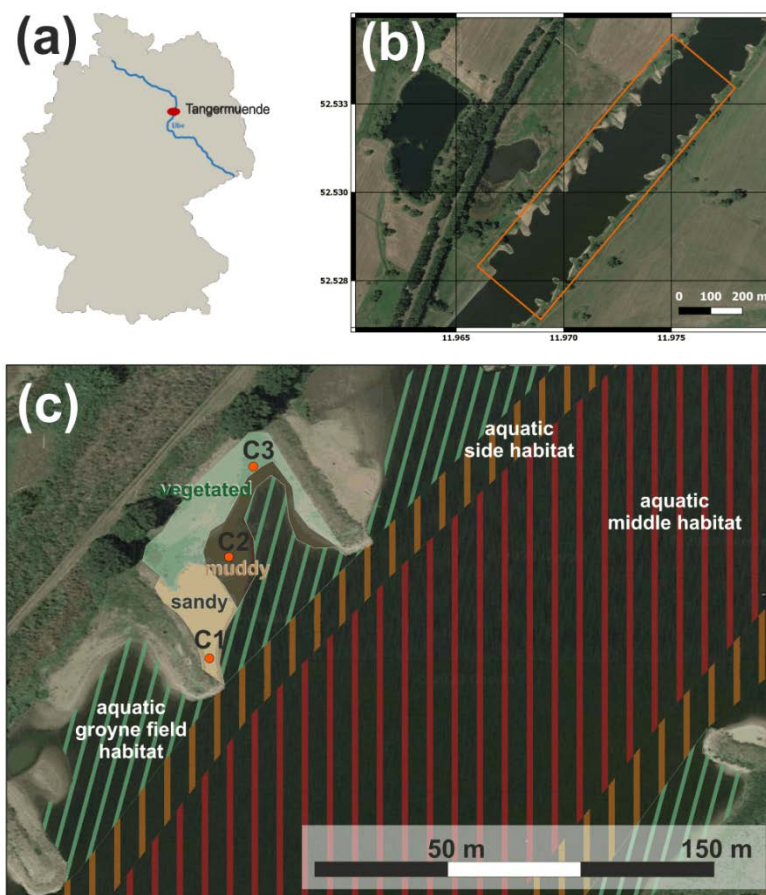
95

Figure 1: Location of the investigation site Tangermünde (red dot) within Germany at River Elbe at river km 388 according to German kilometration (a). Top view of the sampling reach with groyne fields (Source orthophoto: Google Earth, GeoBasis-DE/BKG, date of recording 06/08/2020), flow direction to North-east, study area marked by red lines (b). Detailed view of the study area with indication of habitat types (c). The groyne field is divided into an aquatic habitat and the terrestrial habitat with partially dry fallen sediments, which are divided into sandy areas (location of soil flux chamber C1), muddy areas (chamber C2) and vegetated areas (chamber C3). (Source orthophoto: Google Earth, GeoBasis-DE/BKG, recording date 06/08/2020, © Google Earth, see also Fig. S1).
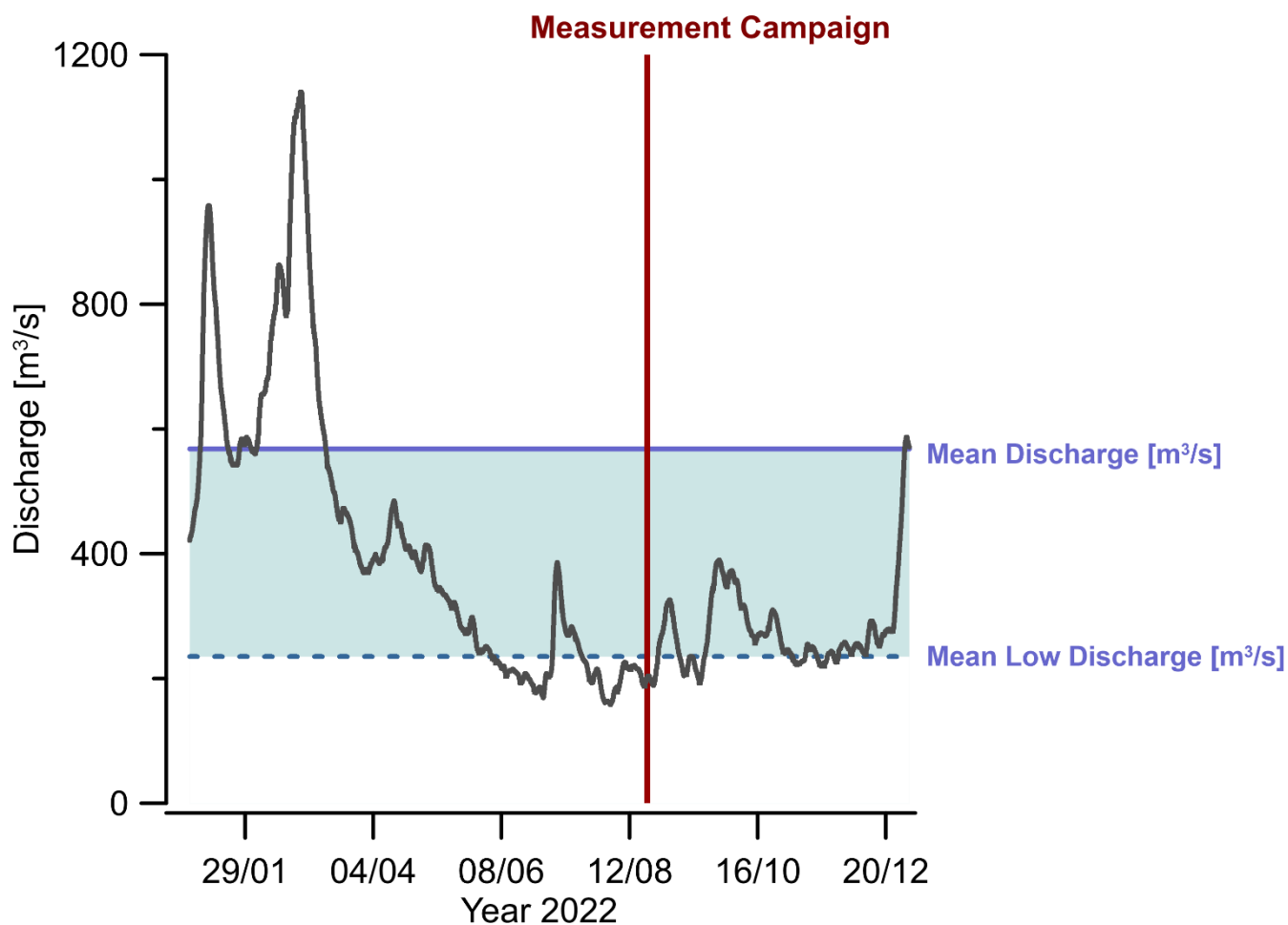
Figure 2: Discharge of River Elbe at gauge Tangermünde during 2022 (German Federal Waterways and Shipping Administration). The blue area marks the range between mean low discharge and mean discharge, the red area marks the period of the sampling campaign.

2.2 Aquatic Measurements

2.2.1 Flow velocity and water depth measurement

Flow velocity profile measurements were conducted at the study site at Tangermünde on 19 August 2022. We deployed a Teledyne RD Instruments (TRDI) four-beam 1200 kHz Rio Grande ADCP[TM] from an inflatable boat. The vertical resolution of water velocities was 0.25 m (25 cm bins), and the sampling frequency was approximately 2 Hz. In total 8 transects of flow velocity and water depth where measured using 4-5 replicates at each transect (Figure S2 in the Supplement). The minimum and maximum measured flow velocity were 0.007 and 1.05 ms^{-1}, and the minimum and maximum water depths were 0.45 and 3.1 m respectively. Depth-averaged velocities (U) were calculated from the measured portion of the water column, neglecting

5

115 the unmeasured upper and lower portion of the water column (see Figure S2 in the Supplement). Global positioning system (GPS) position data were collected using a GPS tracker (Garmin International) with a frequency of 1s.

Basic hydrographic parameters (temperature, conductivity, oxygen, pH, turbidity and chlorophyll) were determined with a pocketferrybox (4Hjena, Kiel, Germany) and a multiparameter probe (Exo2, YSI). The water supply for both sensors was the moon pool of the Albis. We mapped basic hydrographic parameters with the RV Albis meandering between the western and eastern groyne heads on 19 August 2022. Due to the size of the ship, it was not possible to enter near-shore areas and groyne

120 fields. From 19-22 August 2022, the RV Albis was anchored at the pier in Tangermünde and measured the hydrographic parameters at the same position, continuously for 63 hours.

2.2.2 Aquatic GHG measurements

To assess the spatial pattern of aquatic GHG emissions, aquatic GHG fluxes were measured from an inflatable boat using a floating chamber connected to a portable FTIR analyser (GASMET) as explained in Lorke et al. (2015). For each measurement

125 the chamber was deployed from a drifting boat for 2-5 minutes. Fluxes were calculated from the linear change of CO_2 and CH_4 mixing ratios in the chamber. A water sample for later gas chromatograph (GC) analysis was taken during each flux measurement. Surface water samples of 30 mL were taken with 60 mL syringes, and 30 ml of ambient air was added to the syringes, which was then vigorously shaken for one minute. The equilibrated headspace was then transferred to pre-evacuated exetainers and the equilibration temperature was measured in the remaining water sample.

130 Dissolved methane concentrations were mapped with a dissolved gas extraction unit and a laser-based analytical Greenhouse Gas Analyzer (GGA; both Los Gatos Research, United States) on an inflatable boat. The degassing unit withdrew water from the water basin or directly from surface water at 1.2 L min^{-1}. Methane was extracted from the water via a hydrophobic membrane and hydrocarbon-free carrier gas was on the other side of the membrane (nitrogen, at 0.5 L min^{-1}). The carrier gas with the extracted CH_4 was then directed to the inlet of the gas analyser. The time offset between the water intake and stable

135 recording at the GGA was determined beforehand in the laboratory. To convert the relative concentrations (ppm) given by the GGA to absolute concentrations (nmol L^{-1}), discrete water samples were obtained at least every hour. The CH_4 concentration in these bottles was determined using the headspace method and gas chromatographic analysis. Based on the obtained values, the conversion factor (ppm to nmol L^{-1}) of 84.88 was determined.

For high-spatial resolution measurements the instruments were set-up in a small rubber boat with a 5-L nitrogen tank and a car

140 battery. The water inlet of the degasser was fixed to a bar and submerged to approx. 20 cm water depth. We entered each groyne field from the north and kept the boat at the groyne heads for approximately 2 min. (against the current) and then entered the following groyne field as far as possible (Figure 5).

For continuous measurements of dissolved CO_2 and CH_4, an optical AMT-Sensor (Rostock, Germany) and a Contros-Sensor (4H-Jena, Jena, Germany) were deployed in the moon pool of the Albis. The CO_2 sensor provided data as ppm which were

145 converted to concentrations (µmol L^{-1}) according to its solubility at the respective temperature (UNESCO/IHA, 2010). The

CH_4 mixing ratio (ppm) given by the Contros Sensor was corrected to absolute concentrations (µmol L^{-1}) using the CH_4 concentration in water samples taken during the measuring interval and analysed with gas chromatography.

2.3 Terrestrial measurements

The mixing ratio of CO_2 in the atmosphere and other meteorological parameters was continuously measured by a sensebox.
150 The sensebox system is a toolkit developed in the framework of Citizen Science projects for environmental data collection funded by the German Federal Ministry of Education and Research. It consists of an open-source microcontroller unit which can deploy various environmental sensors (Bartoscheck et al., 2019). The sensebox was equipped with a GPS-sensor, an environmental sensor measuring air temperature, relative humidity and air pressure, and a CO_2 - sensor determining the air CO_2 mixing ratio. The sensebox was installed at the RV Albis and measured the atmospheric conditions every 5 minutes.
155 The spatial variability of CO_2 and CH_4 fluxes at terrestrial sediments was measured with the laser-based trace gas analyser LI-7810 (LI-COR Biosciences, USA) in combination with a closed chamber (LI-COR smart chamber). Soil gas fluxes were calculated from the temporal gas concentration change taking into consideration the chamber volume and the surface area of the soil area covered by the chamber. For each sampling point the change in gas concentration in the closed chamber was determined after a purging period in a 1-second sampling interval during the 2-minute observation time. Fluxes were calculated
160 using the linear fitting approach of the SoilFluxPro Software (LI-COR). Based on our own long-term tests with the system, soil flux detection limits were determined for CO_2 of ± 0.36 mmol m^{-2} h^{-1} (corresponding to a change of 2 ppm CO_2 during a closure time period of 2 minutes) and for CH_4 of ± 0.072 µmol m^{-2} h^{-1} (corresponding to a change of 0.6 ppb CH_4 during a closure time period of 2 minutes).

To cover the temporal dynamics of terrestrial CO_2 emissions, three opaque automatic chambers (CFLUX-1 Automated Soil
165 CO_2 Flux System, PP systems, Amesbury, Massachusetts, USA) were installed at a sandy site, a muddy site, and a sandy site with herbaceous vegetation (Figure 1 d). The chambers measured CO_2 fluxes once every hour. Each flux measurement lasted for 5 min, and the chambers were open for 55 min between flux measurements. CO_2 fluxes were calculated from the linear increase of CO_2. The detection limit for terrestrial CO_2 fluxes was 0.08 mmol m^{-2} h^{-1}. Each chamber was equipped with a soil moisture and temperature probe (Stevens HydraProbe, Stevens Water Monitoring Systems, Portland, Oregon, USA).
170 Light intensity was measured at Magdeburg (50 km from Tangermünde) as PAR [µmol m^{-2} s^{-1}] using a LI-190R Quantum Sensor (Licor, Lincoln, U.S.A.).

2.4 Laboratory Analyses

CO_2 and CH_4 concentrations in gas samples were measured with a gas chromatograph (GC) (SRI 8610C, SRI Instruments Europe, Bad Honnef, Germany). The GC was equipped with a flame ionisation detector and a methanizer which allowed for
175 simultaneous measurement of CO_2 and CH_4 with an uncertainty of < 5 %. Dissolved gas concentrations were calculated using

temperature-dependent Henry coefficients (UNESCO/IHA, 2010). CO_2 concentrations were corrected for alkalinity as described in Koschorreck et al. (2021).

2.5 Calculations and Statistics

Gas transfer coefficients were calculated from CH_4 fluxes measured by the floating chambers divided by the difference between

180   actual and equilibrium CH_4 concentration. Equilibrium CH_4 concentrations were calculated from the mean measured atmospheric CH_4 mixing ratio (2.5 ppm) using temperature-dependent Henry coefficients from Sander (2015); (Koschorreck et al., 2021). The so-determined k_{CH4} was converted to k_{600} and k_{CO2} using Schmidt numbers according to UNESCO/IHA (2010). We did not use CO_2 data for k_{600} calculations because the CO_2 concentration was close to equilibrium resulting in large uncertainties in the calculation of k_{600}.

185   Probe measurements of CO_2 and CH_4 concentrations were converted to fluxes using the measured gas transfer velocity of k600 = 5.5 m d^{-1} (Table 1). k600 was converted to kCO2 and kCH4 as explained in Striegl et al. (2012) .

Emissions from different habitat types were compared by pairwise Wilcoxon tests. Fluxes during the day were compared to fluxes during night using Wilcoxon rank sum tests. For statistical analysis, all high-frequency data were transformed to hourly data by calculating the mean values of data available between 30 minutes before and 30 minutes after the full hour. Time series

190   data were log transformed after checking for normality by using Shapiro-Wilk tests. Significance of linear correlation of log transformed fluxes with drivers was checked by F-tests ($p < 0.05$). Mixed linear models to explain GHG fluxes from combinations of predictors were compared based on their AIC. All statistical analyses were done with R (R-Core-Team, 2016).

3 Results

3.1 Hydrodynamic and climatic conditions

195   Our study was conducted during a typical summer low-water situation. At the gauge level of 134 cm (on 6 August 2022, when the orthophoto in Figure 1 was taken), 9 % of the study area was not covered by water (Table 1). Flow velocity in the river was relatively uniform around 0.65 m s^{-1} while within the groyne fields flow velocity was significantly lower (Table 1). Water was flowing rather smoothly without larger waves, but we observed more turbulent conditions downstream of groyne heads. The mean water depth was 1.82 m with the most shallow but also the deepest parts in the groyne fields (maximum depth 3.1

200   m). The water level rose by 10 cm over the 3 days of our study. Weather conditions were rather constant during our study period, predominantly sunny, with 5.6 mm of rainfall during the first night (19.8. until 6 am). Air temperature fluctuated between 12.4° and 32.2° and low wind speeds of 0.3 ± 0.6 m s^{-1} were recorded. Water temperatures were evenly distributed (23.3 ± 0.04°C, measured between 19.08.2022 14:00 and 22.08.2022 08:00). Electrical conductivity of the water at the western shore and within the western groyne fields was about 200 µS cm^{-1} higher than on the eastern shore (Fig. S3). This conductivity

205 gradient has been attributed to the salty inflow of river Saale 97 km upstream of our sampling site (Weigold and Baborowski, 2009). It indicates limited lateral mixing of river water even over a large distance.

3.2 Spatial variability

GHG concentrations and emissions differed between habitats and also between the two gases CO_2 and CH_4 (Table 1). The water was over-saturated both with CO_2 and CH_4, resulting in positive fluxes (= emission to the atmosphere). The flux of CO_2

210 from the water surface was two orders of magnitude higher than the CH_4 flux. Dissolved CO_2 concentrations were highest in the middle of the river and decreased towards the side. An opposite pattern was observed for CH_4 which was higher at the side and within the groyne fields than in the middle of the river (Figure 3). Since the gas transfer velocity k600 was twice as high at the sites compared to the middle of the river, CH_4 emissions were significantly higher at the side and in the groyne field compared to the middle of the river. Since higher CO_2 concentrations in the middle of the river were compensated by lower

215 k600 values, emissions of CO_2 did not differ significantly between aquatic habitats (Figure 4).

The dry habitats had higher CO_2 emissions but lower CH_4 emissions compared to the aquatic sites. Dry CO_2 emissions showed a large variability within habitats and were highest at vegetated sites and very low at the sandy sites (Figure 4). Dry CH_4 emissions, in contrast, were more than two orders of magnitude lower, in some cases even slightly negative (Table 1), and only small differences between habitats were observed.
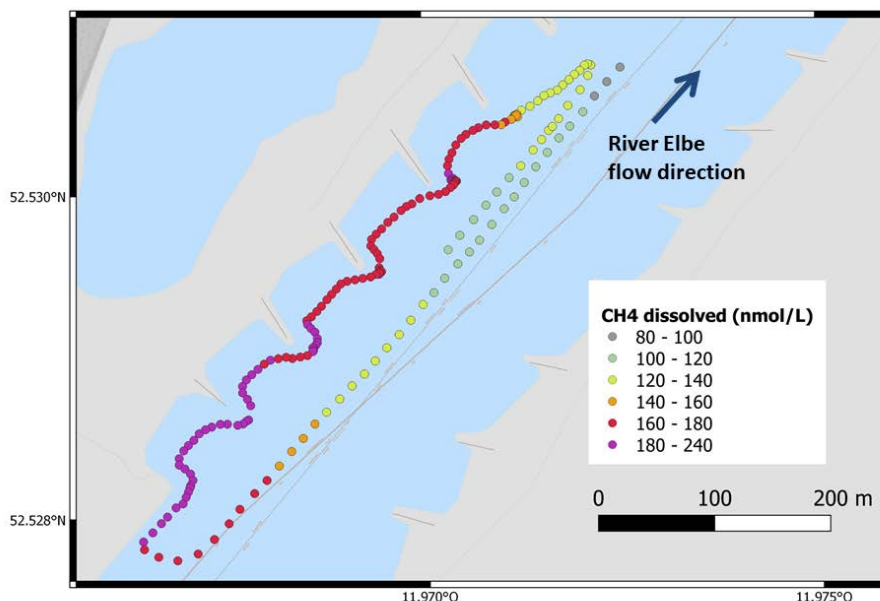

220

Figure 3: Concentrations of dissolved CH4 in the water measured continuously with a mobile gas extraction unit connected to a GHG analyser. Measurements were carried out from an inflatable boat on 21.8.2022 between 16:18 and 16:51.

Table 1: GHG emissions and their regulating factors in different habitat types. Emission data from floating chamber
225 measurements, CH_4 concentration measured by a membrane equilibrator connected to a portable GHG analyser (data from
Figure 3), CO_2 concentration analysed by GC, velocity measured by ADCP. Areas were manually extracted from a recent
Google earth image (Figure 1). all data: median (range). CH_4 fluxes are given in $\mu mol\ m^{-2}\ h^{-1}$ and CO_2 fluxes in $mmol\ m^{-2}\ h^{-1}$.

	aquatic			terrestrial		
	middle	side	groyne fields	sandy	muddy	vegetated
CH_4 emissions [$\mu mol\ m^{-2}\ h^{-1}$]	12.2 (6-20.7)	24.9 (6-73)	39 (12.6-52.6)	0.2 (-0.06 - 0.45)	0.1 (-0.8 - 2.5)	-0.1 (-2.8 - 0.4)
CO_2 emissions [$mmol\ m^{-2}\ h^{-1}$]	2.2 (1.86-2.21)	1.5 (1.07-3.14)	0.8 (0.21-2.3)	0.6 (0.4 - 1.3)	1.3 (-1.5 - 3.9)	2.8 (0.2 - 13.9)
CH_4 concentration [$\mu mol\ L^{-1}$]	0.12 (0.11 - 0.16)	0.18 (0.17 - 0.32)	0.18 (0.17 -0.21)	-	-	-
CO_2 concentration [$\mu mol\ L^{-1}$]	29.3 (28.4-29.6)	23.4 (15.4-24.3)	15.7 (15.4-28.8)	-	-	-
k600 [$m\ d^{-1}$]	2.8 (1.7-5.5)	5.7 (2.3-10.8)	4.9 (1.5-6)	-	-	-
velocity [$m\ s^{-1}$]	0.79 (0.72-0.81)	0.65 (0.22-0.84)	0.22 (0.09-0.45)	-	-	-
total area [m^2]	125,000	25,000	42,000	7,700	4,800	6,500
total CH_4 emissions [$mol\ h^{-1}$]	1.5 (0.7 - 2.6)	0.6 (0.1 - 1.8)	1.6 (0.5 - 2.2)	0.0015 (-0.0005 - 0.0035)	0.0005 (-0.0038 - 0.012)	-0.00065 (-0.018 - 0.0026)
total CO_2 emissions [$mol\ h^{-1}$]	275 (232 - 276)	37.5 (26.7 - 78.5)	33.6 (8.8 - 96.6)	4.6 (3.1 - 10.0)	6.2 (-7.2 - 18.7)	18.2 (1.3 - 90.3)
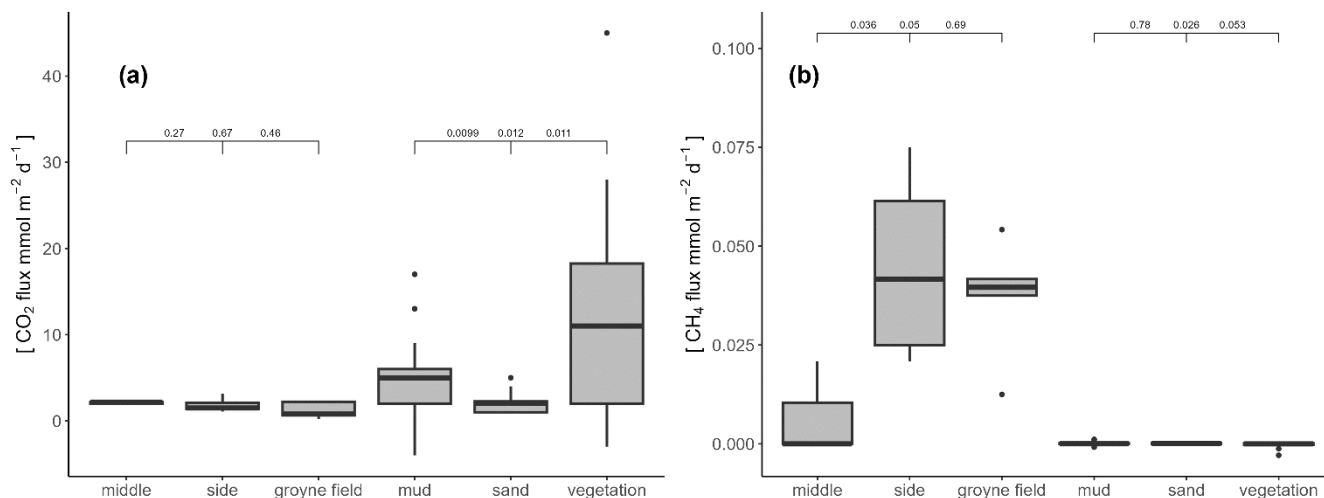
230

Figure 4: Boxplots comparing CO_2 flux (a) and CH_4 flux (b) in different habitat types. Numbers within the plots indicate p-values of pairwise comparisons using Wilcoxon tests.

3.3 Temporal variability

Continuous measurements of aquatic GHG concentrations (Figure S4) and water physicochemical variables were carried out

235 over a period of 2.5 days at the side of the river. Water temperature (median 22.6; range 21.7 - 23.7°C), pH (median 8.0; range 7.3 - 8.3) and oxygen (median 97.9; 87.5 - 117.8 % saturation) showed a clear daily pattern, with lowest values in the early morning (5:00 - 6:00), while conductivity was rather constant (median 1260; range 1146 - 1381 µS/cm; Supp. Figure S5).

Aquatic CO_2 concentrations showed a clear diurnal cycle with rising concentrations during the night and decreasing concentrations during the day. The diurnal amplitude of the resulting flux spanned about 5 mmol m² h^{-1} with maximum fluxes

240 around 7:00 and minimum fluxes around 17:00 (blue line in Figure 5a). In contrast to CO_2, the CH_4 concentration and the flux did not change with time (Figure 5b).

At the dry sites diurnal pattern of CO_2 emissions are apparent, but these patterns differed between habitat type. At the vegetated site a pattern similar to the aquatic site was observed, but phase shifted. The highest fluxes were found around noon, while the minimum was at 4:00 before sunrise (green line in Figure 5a). The mud site did not show such a sinus-like pattern but rather

245 a two-state pattern: The site switched from constant emissions during the night to constant CO_2 uptake during the day (red line in Figure 5a). No diurnal variability of CO_2 emissions was observed at the sandy site (yellow line in Figure 5a). The CH_4 flux data from the dry sites do not allow visualisation of diurnal variability, but the data (dots in Figure 5b) at least do not show any temporal trend during the day.

CO_2 emissions from the mud and the vegetated site showed a decreasing trend during our study. At the muddy site this trend

250 was associated with increasing sediment moisture (Figure 5c), which was obviously caused by the rising water level of the

river (Figure 5d) - on 21.8. the flux chamber was only 1 m from the water line. At the other dry sites no trend of sediment moisture was visible, but sediment temperature during the day tended to increase through the study (Figure 5c).
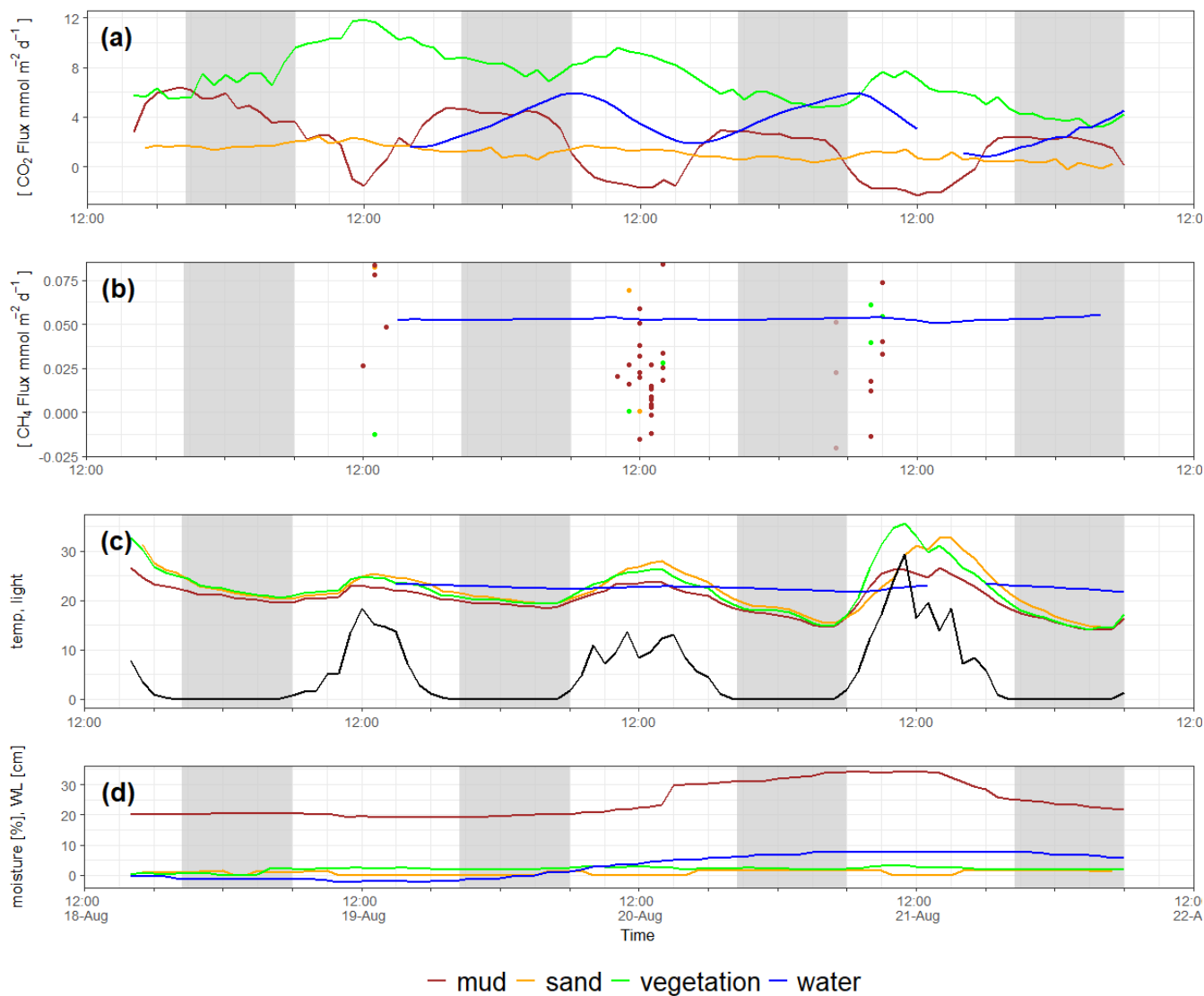
Figure 5: Time series of CO_2 flux (a), CH_4 flux (b), sediment and water temperature (c), and sediment moisture and water level (d).
All data with hourly resolution. Black line in c) shows light measured as PAR [μmol m^{-2} s^{-1}/2]. Grey-shaded areas indicate night.

As a result of these diurnal patterns, fluxes were significantly higher during the day than during the night at the sandy and vegetated site, while at the muddy site fluxes were higher at night than during daylight (Table 2). At the water site, medians did not differ significantly between day and night.

We tried to correlate the dry CO_2 flux with measured potential drivers (Figure S6). The CO_2 flux was weakly negatively correlated with sediment moisture and water level. Correlation with temperature or light (which were highly auto-correlated)

including all data was not significant (F-test, p>0.05), which is consistent with the observed different diurnal pattern at different sites. Furthermore, the temperature of the water was relatively constant – in contrast to the dry sites where diurnal temperature amplitudes up to 20° were observed (Figure 5c). If we correlate the CO_2 flux with temperature or light for each habitat type separately, we get a significant positive correlation at the sandy and vegetated site, while the correlation was negative at the

265   muddy site (Figure S7). A positive correlation with light was observed at the vegetated site, while the correlation was negative at the muddy site.

To consider site-specific correlations, we added site as a random factor to our statistical model. A mixed linear model with (log-transformed) temperature, light, water level, and sediment moisture as fixed factors and site as random factor explained 82 % of the variability. The best-simplified model (based on AIC) contained water level and sediment moisture as fixed factors

270   and had a conditional R^2 of 0.82.

Table 2: Median (range) of temporal GHG fluxes at different sites (data from Figure 7). Day and night separated by sunrise/sunset. Day and night data were significantly different for the dry sites but not for the water (Wilcox test).

	habitat	all data	day	night
CO_2 flux	mud	2.3 (-2.34 - 6.41)	0.07 (-2.34 - 6.16)	2.97 (1.3 - 6.41)
	sand	1.19 (-0.22 - 2.45)	1.37 (0.43 - 2.45)	0.79 (-0.22 - 1.91)
	vegetation	7.06 (3.24 - 11.84)	8.17 (4.21 - 11.84)	6.01 (3.24 - 8.75)
	water	3.32 (0.80 - 5.96)	2.94 (0.80 - 5.96)	3.53 (1.26 - 5.77)
CH_4 flux	water	0.052 (0.05 - 0.055)	0.053 (0.05 - 0.054)	0.053 (0.052 - 0.055)

275   **3.4 Comparison of spatial and temporal variability**

We calculated coefficients of variation (CV) to make spatial and temporal variability comparable (Figure 6). Consistent with our hypothesis, spatial variability of CH_4 emissions had a higher CV compared to CO_2 both in aquatic and dry habitats. Also consistent with our hypothesis, temporal variability of the CO_2 flux had a higher CV than CH_4 flux at the aquatic sites. At the dry sites (where we did not measure temporal changes in CH_4 flux) the temporal variability of the CO_2 flux also showed a high

280   CV. If we want to judge the consequences of this result on upscaling, however, the absolute height of the fluxes as well as the relative areas of the different habitats need to be considered.

13
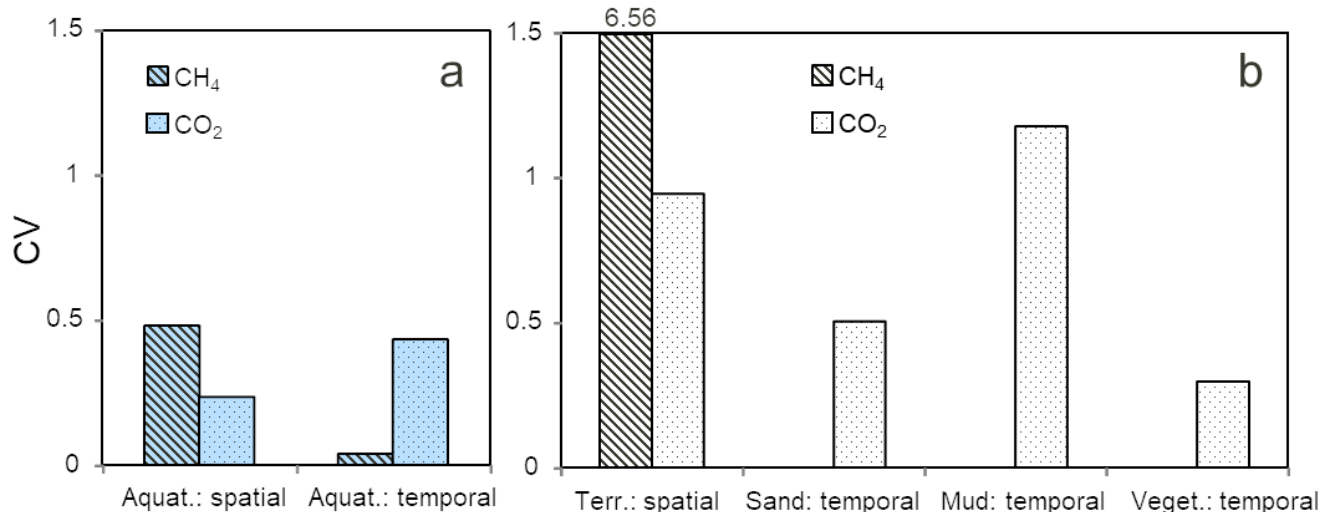
Figure 6: Coefficients of variation of spatial (calculated from Table 1) and temporal (calculated from Figure 5) variability of CH$_4$ fluxes and CO$_2$ fluxes of aquatic sites (a) and dry sites (b) accordingly. Temporal variability of CH$_4$ fluxes from terrestrial sites was not calculated.

3.5 Upscaling

About 10 % of our study area was not covered by water (Table 1). Within the dry area, all three habitat types contributed similarly to the total area. If we apply a "perfect" approach considering spatial variability of CH$_4$ and both spatial and temporal variability for CO$_2$, our study reach emitted 91 mol CH$_4$ d^{-1} and 16962 mol CO$_2$ d^{-1} (Table 3). Thus, CH$_4$ contributed 5 % to total CO$_2$-eq emissions. GHG emissions were dominated by the aquatic habitats which contributed 91 % to the total emissions. CH$_4$ emissions from terrestrial habits can be neglected, while at the aquatic habitats they contributed about 6 % to the CO$_2$-eq emissions.

Table 3: Total GHG emissions from our studied reach quantified considering both spatial and temporal variability. For CO$_2$ emissions we multiplied the median flux from the temporal data (Figure 5) by habitat areas (Table 1). For aquatic CO$_2$ emissions, the temporal median flux at the side was also applied to the other aquatic habitats. For CH$_4$ emissions we used the spatially different fluxes (Table 1). For CO$_2$-eq the CH$_4$ emissions were converted to CO$_2$-eq using a GWP of 28 and added to the CO$_2$ emissions.

	aquatic				terrestrial				all
	middle	side	groyne fields	total	sandy	muddy	vegetated	total	total
CH$_4$ [mol d^{-1}]	36.6	14.94	39	91	0.018	0.023	-0.016	0	91
CO$_2$ [mol d^{-1}]	9960	1992	3347	15299	425	137	1101	1663	16962
CO$_2$-eq [mol d^{-1}]	10333	2144	3747	16224	425	137	1101	1664	17887

Biogeosciences
Discussions

4 Discussion

4.1 Spatial variability

Our results show considerable spatial variability of CH_4 emissions from aquatic sites. This confirms earlier observations (Staniek, 2018) and can be explained by the fact that CH_4 is primarily produced in the sediment and thus, depends on the spatial heterogeneity of the sediments. Sediment deposition in rivers is highly heterogeneous and depends on hydrodynamics (Henning and Hentschel, 2013). Fine material rich in organic matter preferably settles at low stream velocity, in our case in the groyne fields. Thus, our study confirms the hypothesis that the groyne fields are the major source of CH_4 in river Elbe (Bussmann et al., 2022).

The data also revealed a significant difference between aquatic and terrestrial CH_4 emissions. CH_4 emissions from dry sediments have rarely been measured, and there is still debate about their significance. A recent global survey indicates that these CH_4 emissions probably cannot be neglected (Paranaíba et al., 2021). However, our results confirm previous observations that CH_4 emissions from dry river sediments are rather small compared to CO_2 emissions (Koschorreck et al., 2022). It has been suggested that there might be local hot spots of CH_4 emissions (Marcé et al., 2019), but our measurements did not show any evidence for such hot spots.

We also observed considerable spatial variability in the CO_2 concentration in the water. Concentrations were lower in the groyne fields, most probably because of higher photosynthetic activity and higher plankton biomass (Pusch and Fischer, 2006). However, different CO_2 concentrations did not translate into spatial differences in CO_2 emissions, because higher CO_2 concentrations were accompanied by lower gas transfer velocities. This highlights the interacting role of both concentration and gas transfer velocity in shaping spatial patterns of GHG emissions from rivers.

While spatial differences in concentrations have already been acknowledged (Bussmann et al., 2022) our study is, to our knowledge, the first to show small-scale spatial differences in gas transfer velocities in a river. Measuring k_{600} in rivers is not an easy task, because tracer addition approaches, as typically used in small streams (Hope et al., 2001), cannot be applied. The floating chamber method is probably the only existing method that can be used in intermediate to large streams (Lorke et al., 2015). The spatial resolution of the method depends on the duration of the measurement, because the boat is drifting during the measurement. We tried to minimise measuring time to about 2 minutes to optimise spatial resolution. Thus, at the measured flow velocity of 0.8 m s^{-1}, a typical flux measurement spanned a drift path of about 100m, which might be the limit for the spatial resolution in the direction of the flow. Since we were drifting parallel to the shore, however, the method was well suited to distinguish k_{600} between the middle and side of the river. While higher k_{600} values at the side of the river were expected, the high k_{600} in the groyne fields are somehow surprising. This indicates that factors like bottom roughness and flow energy dissipation at the banks had a larger effect on turbulence on k than simply flow velocity (which was higher in the middle of the stream). Wind was not an important factor controlling k_{600} values in our study because wind speeds were low and rather constant. It can be expected that in larger and winding rivers with variable fetch, wind field heterogeneities further contribute to the spatial variability of k_{600}. It is reasonable to assume that spatially variable gas transfer velocities should also be

considered in stream metabolism calculations where k600 is used to quantify oxygen exchange between water and atmosphere (Demars et al., 2015).

335 Compared to the aquatic sites, the CO_2 emissions from terrestrial sites showed considerable inter-habitat variability. Higher CO_2 emissions from darker (= more muddy) sites compared to sandy sites have been used to scale up CO_2 emissions from dry river sediments using remote sensing (Mallast et al., 2020). They can be explained both by higher organic matter content of the muddy sediments as well as higher sediment moisture which favors microbial CO_2 production in the sediment (Keller et al., 2020). However, the observed trend of decreasing CO_2 emissions with increasing sediment moisture (Figure 5) shows that wetter conditions not necessarily result in higher fluxes. CO_2 emissions from muddy sediments obviously result from a

340 complex interplay between organic matter availability and moisture dependent gas transport limitation (Keller et al., 2020).

The sediment in the proximity of terrestrial vegetation showed clearly elevated CO_2 emissions, confirming earlier observations (Bolpagni et al., 2017; Koschorreck et al., 2022). Since we excluded plants from our chambers, these elevated CO_2 emissions are probably caused by root respiration. It is well known that in soils root respiration contributes about 50 % to soil respiration (Hanson et al., 2000). It is clear that at vegetated sites our CO_2 fluxes cannot be equated with net ecosystem exchange because

345 the plants were excluded from our chambers. To fully assess the effect of terrestrial plants on river CO_2 emissions, measurements using transparent chambers and considering light conditions as well as plant biomass determinations are necessary. The exclusion of plants from our measurements means that we systematically overestimate CO_2 emissions from vegetated sites in the growing season. However, we argue that this bias might be small in our study when CO_2 uptake by the plants during the day was probably largely compensated by higher CO_2 emissions due to plant respiration during the night.

350 Taken together, our results show that spatial differences were especially apparent for CH_4. The terrestrial habitats need to be considered for CO_2 emissions while they can probably be neglected for ecosystem-scale CH_4 emissions from river Elbe.

4.2 Temporal variability of CO_2 and CH_4

Our results confirm that diurnal variability of CO_2, which has been shown in streams (Attermeyer et al., 2021; Gómez-Gener et al., 2021) as well as marine systems (Honkanen et al., 2021), is also relevant in rivers. Interestingly, the shape of the diurnal

355 curve of CO_2 emissions differed between habitats, showing that different regulatory mechanisms are at play.

At aquatic sites biological fixation and mineralization of carbon led to sinusoidal diurnal pCO_2 variations, with a maximum in the morning and a minimum in the afternoon. This pattern was obviously driven by light since the diurnal temperature amplitude in the water was below 1.5°C.

The temporal pattern at the muddy site was also most likely driven by the interplay between microalgae primary production

360 and respiration, but the shape of the diurnal CO_2 curve differed considerably. These data nicely demonstrate that the same regulatory mechanism (light-dependent balance of photosynthesis and respiration) may result in different diurnal pattern depending on the physical environments. In water, changes in biological activity are buffered by the DIC pool in the water, resulting in gradual changes of CO_2 concentration during the day. At terrestrial sites, switching photosynthesis on and off

changes the sediment from a CO_2 sink to a source and back again. Since microbial respiration depends on temperature and
365 temperature fluctuations in the sediment were quite large, it is somewhat surprising that we did not see a pronounced
temperature signal in the CO_2 flux (as in Koschorreck et al. (2022)). A possible explanation is that the CO_2 pool in the pore
space buffers the effect of fluctuating respiration. Since the flux of CO_2 between the sediment and the atmosphere is driven by
the concentration gradient, this results in rather constant CO_2 efflux during the night. During the day this efflux is most
probably blocked by photosynthetic uptake of CO_2 by benthic microalgae. In a laboratory study with marine sediments, a
370 similar fast switching process between plateau-like CO_2 production in the dark and CO_2 uptake during the light, was observed
(Tang and Kristensen, 2007). Detailed investigations of benthic primary production on exposed marine sediments showed that
both linear and plateau relationships were obtained between the fluorescence parameter (relative electron transport rate [rETR])
and the community-level carbon-fixation rate (Migne et al., 2007). The reason for a "Plateau behavior" was the migration of
some cells to greater depth in order to avoid too much light. Possible physiological explanations might be the existence of
375 alternative electron sinks (e.g., the Mehler reaction or photorespiration) or limitation by Calvin cycle reactions.

At vegetated sites, the diurnal pattern was probably driven by diurnal fluctuating plant metabolism and root respiration.
However, the diurnal CO_2 flux curve was not in phase with the light or temperature curve. This can be explained by a hysteresis
effect caused by the transit time of CO_2 from the source of its formation (probably the plant roots) and the sediment surface
(Koschorreck et al., 2022; Phillips et al., 2011).

380 Diurnal variability of CH_4 emissions was observed in a study focussing on spatio-temporal variability of GHG emissions in
the Danube Delta (Canning et al., 2021). Elevated CH_4 emissions from a floodplain lake and a channel were attributed to
stratification and temporary mixing of the water column. In our case the water column was permanently mixed and diurnal
variability was not an issue for CH_4 fluxes. Methane is produced in deeper sediment layers and, thus, is not affected by light
driven changes of redox conditions at the very sediment surface. Even if CH_4 oxidation at the sediment surface were affected
385 by phototrophic activity, this would not result in fluctuating emissions because these are buffered by the CH_4 pool in the water.
Thus, we have confirmed our hypothesis that diurnal variability is relevant for CO_2 but not for CH_4. We also show that the
shape of the diurnal CO_2 flux curve depends on the habitat. As already acknowledged in the literature, this has important
implications for monitoring strategies and upscaling (Gómez-Gener et al., 2021).

4.3 Implications for measurement strategy and upscaling

390 Based on our results, the best monitoring strategy for our stream reach should consider spatial variability of CH_4 and both
spatial and temporal variability of CO_2. Applying that approach to our data (Table 3) revealed the dominant role of CO_2 (due
to low CH_4 fluxes) and aquatic habitats (due to their larger area).

It is evident that the exact quantification of habitat areas is crucial. Stream surface areas are typically estimated from empirical
relations depending on stream order (Raymond et al., 2012) or remote sensing (Palmer and Ruhi, 2018). Estimating river width
395 from annual mean discharge, according to Raymond et al. (2012), reveals in our case a width of 183m. This is very similar to

the mean width of our reach of 200 m, which we obtain by dividing the water surface area (Table 1) by reach length (0.96 km). Although we found good agreement between measured widths and those calculated using the equation of Raymond et al. (2012), measured flux widths should always be used for field studies because of the large scatter in the regression and the logyrhytmic scale used. Thus, if stream width is not explicitly measured, expected errors can become considerably larger than

400   the standard error. These approaches, however, do not include dry sediment areas. In our case 9 % of the total area was dry, which is somewhat lower than the 26 % estimated from remote sensing data during the extreme drought in 2018 (Mallast et al., 2020). During that drought, dry sediment areas showed clear longitudinal variability along the river depending on topography ranging from 2 % to 40 % of the river area being dry. A straightforward strategy would be to determine dry areas for different discharge scenarios to derive a quantitative relation between dry area, water area, and discharge.

405   We used our dataset to simulate different monitoring approaches and compared them with the optimal approach (Figure 7). Only sampling the river during the day at the side would result in more than 50 % under estimation of the real GHG emissions – mostly because higher CO_2 emissions during the night are not considered. Measuring in the middle of the river or even in all habitats during the day would only slightly improve the result. If both CO_2 and CH_4 emissions were measured over a 24 h cycle only along the side of the river, we would slightly overestimate emissions because of high CH_4 emissions along the side.

410   The convenient approach of deploying only a CO_2 probe at the side of the river would result in about 5 % underestimation of total CO_2-eq emissions from our study reach.
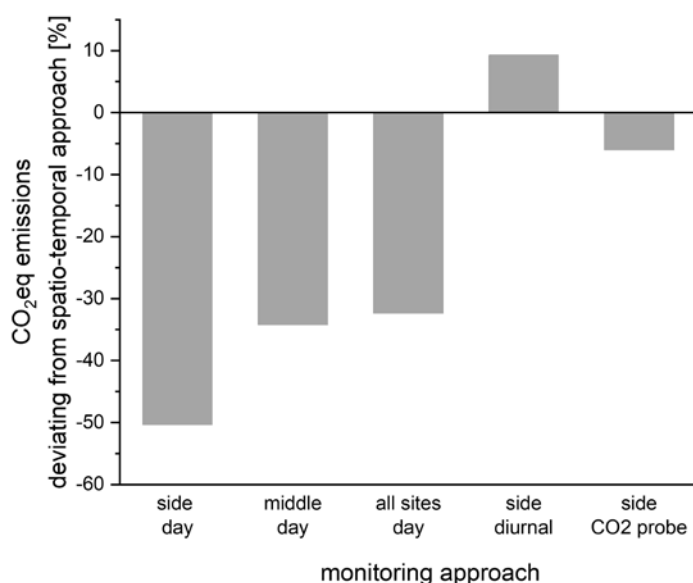
Figure 7: Deviation of total GHG emissions (CO_2-eq) obtained by different monitoring approaches from perfect approach (spatial
415   **variability of CH_4 and both spatial and temporal variability of CO_2 considered).**

However, these considerations differ depending on the target gas. If we sample only during the day along the side of the river, for example, we would underestimate CO_2 emissions by about 50 % but overestimate CH_4 emissions by 40 % (Figure S8). Although our results reveal some general principles, they cannot be simply applied to other systems. For the design of a perfect monitoring strategy for a given river, the particular habitat types and diversity need to be considered. We can also expect that

420 the role of spatial and temporal variability changes with the season, both because habitat areas and regulatory factors like temperature or day-length change (Koschorreck et al., 2022). We would also expect that CH_4 variability needs to be re-assessed if ebullition becomes relevant (Maeck et al., 2014), especially in dammed river sections (Matoušů et al., 2019) or floodplain waters and under warm conditions (Barbosa et al., 2021). More natural river-floodplain systems containing floodplain lakes are known to harbour extreme spatial variability with significant CH_4 emissions (Maier et al., 2021), calling for a more

425 sophisticated monitoring approach (Canning et al., 2021).

4.4 Conclusion

Although we only provide a snapshot case study at a German river, we can derive a number of conclusions relevant for the quantification of GHG emission from large temperate rivers.

It is now evident from several studies that continuous measurements are necessary to come up with realistic emission

430 approaches. CO_2 probes are becoming more and more popular. Deploying them in numerous rivers will improve global riverine CO_2 emissions estimates.

It is also clear that river sediments drying up at low discharge need to be considered at least for CO_2 budgets. However, when it comes to total GHG emissions, lower CH_4 emissions compensate for higher CO_2 emissions from dry sediments; this is a scenario already hypothesised for reservoir sediments (Marcé et al., 2019).

435 Finally, our data show that anthropogenic modification of the river (here: the construction of groynes) has the potential to alter GHG emissions significantly. In our case, the groyne fields nearly doubled CH_4 emissions from the river.

Competing Interests

The contact author has declared that none of the authors has any competing interests

Acknowledgements

445 framework of MOSES (Modular Observation Solutions for Earth Systems) and the POF-4 topic "Coastal Transition Zones under Natural and Human Pressure".

References

Attermeyer, K., Casas-Ruiz, J. P., Fuss, T., Pastor, A., Cauvy-Fraunié, S., Sheath, D., Nydahl, A. C., Doretto, A., Portela, A. P., Doyle, B. C., Simov, N., Gutmann Roberts, C., Niedrist, G. H., Timoner, X., Evtimova, V., Barral-Fraga, L., Bašić, T., Audet, J., Deininger, A., Busst,
450 G., Fenoglio, S., Catalán, N., de Eyto, E., Pilotto, F., Mor, J.-R., Monteiro, J., Fletcher, D., Noss, C., Colls, M., Nagler, M., Liu, L., Romero González-Quijano, C., Romero, F., Pansch, N., Ledesma, J. L. J., Pegg, J., Klaus, M., Freixa, A., Herrero Ortega, S., Mendoza-Lera, C., Bednařík, A., Fonvielle, J. A., Gilbert, P. J., Kenderov, L. A., Rulík, M., and Bodmer, P.: Carbon dioxide fluxes increase from day to night across European streams, Communications Earth & Environment, 2, 118, 10.1038/s43247-021-00192-w, 2021.
Barbosa, P. M., Melack, J. M., Amaral, J. H. F., Linkhorst, A., and Forsberg, B. R.: Large Seasonal and Habitat Differences in Methane
455 Ebullition on the Amazon Floodplain, Journal of Geophysical Research: Biogeosciences, 126, e2020JG005911, https://doi.org/10.1029/2020JG005911, 2021.
Bartoscheck, T., Fehrenbach, D., and Fehrenbach, J.: Das sensebook-Buch - 12 Projekte rund um Sensoren, dpunkt Verlag, Heidelberg, 2019.
Battin, T. J., Lauerwald, R., Bernhardt, E. S., Bertuzzo, E., Gener, L. G., Hall, R. O., Hotchkiss, E. R., Maavara, T., Pavelsky, T. M., Ran,
460 L., Raymond, P., Rosentreter, J. A., and Regnier, P.: River ecosystem metabolism and carbon biogeochemistry in a changing world, Nature, 613, 449-459, 10.1038/s41586-022-05500-8, 2023.
Bolpagni, R., Folegot, S., Laini, A., and Bartoli, M.: Role of ephemeral vegetation of emerging river bottoms in modulating CO_2 exchanges across a temperate large lowland river stretch, Aquat Sci, 79, 149-158, 10.1007/s00027-016-0486-z, 2017.
Bolpagni, R., Laini, A., Mutti, T., Viaroli, P., and Bartoli, M.: Connectivity and habitat typology drive CO_2 and CH_4 fluxes across land–
465 water interfaces in lowland rivers, Ecohydrology, 12, e2036, doi:10.1002/eco.2036, 2019.
Bussmann, I., Koedel, U., Schütze, C., Kamjunke, N., and Koschorreck, M.: Spatial Variability and Hotspots of Methane Concentrations in a Large Temperate River, Frontiers in Environmental Science, 10, 10.3389/fenvs.2022.833936, 2022.
Canning, A., Wehrli, B., and Körtzinger, A.: Methane in the Danube Delta: the importance of spatial patterns and diel cycles for atmospheric emission estimates, Biogeosciences, 18, 3961-3979, 10.5194/bg-18-3961-2021, 2021.
470 Demars, B. O. L., Thompson, J., and Manson, J. R.: Stream metabolism and the open diel oxygen method: Principles, practice, and perspectives, Limnol Oceanogr-Meth, 13, 356-374, 10.1002/lom3.10030, 2015.
Gómez-Gener, L., Obrador, B., von Schiller, D., Marce, R., Casas-Ruiz, J. P., Proia, L., Acuna, V., Catalan, N., Munoz, I., and Koschorreck, M.: Hot spots for carbon emissions from Mediterranean fluvial networks during summer drought, Biogeochemistry, 125, 409-426, 10.1007/s10533-015-0139-7, 2015.
475 Gómez-Gener, L., Rocher-Ros, G., Battin, T., Cohen, M. J., Dalmagro, H. J., Dinsmore, K. J., Drake, T. W., Duvert, C., Enrich-Prast, A., Horgby, Å., Johnson, M. S., Kirk, L., Machado-Silva, F., Marzolf, N. S., McDowell, M. J., McDowell, W. H., Miettinen, H., Ojala, A. K., Peter, H., Pumpanen, J., Ran, L., Riveros-Iregui, D. A., Santos, I. R., Six, J., Stanley, E. H., Wallin, M. B., White, S. A., and Sponseller, R. A.: Global carbon dioxide efflux from rivers enhanced by high nocturnal emissions, Nature Geoscience, 14, 289-294, 10.1038/s41561-021-00722-3, 2021.
480 Hanson, P. J., Edwards, N. T., Garten, C. T., and Andrews, J. A.: Separating root and soil microbial contributions to soil respiration: A review of methods and observations, Biogeochemistry, 48, 115-146, Doi 10.1023/A:1006244819642, 2000.
Henning, M., and Hentschel, B.: Sedimentation and flow patterns induced by regular and modified groynes on the River Elbe, Germany, Ecohydrology, 6, 598-610, 10.1002/eco.1398, 2013.
Honkanen, M., Müller, J. D., Seppälä, J., Rehder, G., Kielosto, S., Ylöstalo, P., Mäkelä, T., Hatakka, J., and Laakso, L.: The diurnal cycle
485 of pCO_2 in the coastal region of the Baltic Sea, Ocean Sci., 17, 1657-1675, 10.5194/os-17-1657-2021, 2021.
Hope, D., Palmer, S. M., Billett, M. F., and Dawson, J. J. C.: Carbon dioxide and methane evasion from a temperate peatland stream, Limnol Oceanogr, 46, 847-857, 2001.
IPCC: Climate Change 2021: The Physical Science Basis. Contribution of Working Group I to the Sixth Assessment Report of the Intergovernmental Panel on Climate Change, edited by: Masson-Delmotte, V., Zhai, P., Pirani, A., Connors, S. L., Péan, C., Berger, S.,
490 Caud, N., Chen, Y., Goldfarb, L., Gomis, M. I., Huang, M., Leitzell, K., Lonnoy, E., Matthews, J. B. R., Maycock, T. K., Waterfield, T., Yelekçi, O., Yu, R., and Zhou, B., Cambridge University Press, Cambridge, United Kingdom and New York, NY, USA, 2021.
Keller, P. S., Catalán, N., von Schiller, D., Grossart, H. P., Koschorreck, M., Obrador, B., Frassl, M. A., Karakaya, N., Barros, N., Howitt, J. A., Mendoza-Lera, C., Pastor, A., Flaim, G., Aben, R., Riis, T., Arce, M. I., Onandia, G., Paranaíba, J. R., Linkhorst, A., del Campo, R., Amado, A. M., Cauvy-Fraunié, S., Brothers, S., Condon, J., Mendonça, R. F., Reverey, F., Rõõm, E. I., Datry, T., Roland, F., Laas, A.,
495 Obertegger, U., Park, J. H., Wang, H., Kosten, S., Gómez, R., Feijoó, C., Elosegi, A., Sánchez-Montoya, M. M., Finlayson, C. M., Melita,

M., Oliveira Junior, E. S., Muniz, C. C., Gómez-Gener, L., Leigh, C., Zhang, Q., and Marcé, R.: Global CO_2 emissions from dry inland waters share common drivers across ecosystems, Nature Communications, 11, art. 2126, https://doi.org/10.1038/s41467-020-15929-y, 2020.

Kleinwächter, M., Schröder, U., Rödiger, S., Hentwchel, B., and Anlauf, A.: Buhnen in der Elbe und ihre Umgestaltung, in: Alternative Buhnenformen in der Elbe - hydraulische und ökologische Wirkungen, Schweizerbart, Stuttgart, 2017.

500 Koschorreck, M., Prairie, Y. T., Kim, J., and Marce, R.: Technical note: CO_2 is not like CH_4 - limits of and corrections to the headspace method to analyse pCO_2 in fresh water, Biogeosciences, 18, 1619-1627, 10.5194/bg-18-1619-2021, 2021.

Koschorreck, M., Knorr, K. H., and Teichert, L.: Temporal patterns and drivers of CO_2 emission from dry sediments in agroyne field of a large river, Biogeosciences, 19, 5221-5236, 10.5194/bg-19-5221-2022, 2022.

Liu, S., Kuhn, C., Amatulli, G., Aho, K., Butman, D. E., Allen, G. H., Lin, P., Pan, M., Yamazaki, D., Brinkerhoff, C., Gleason, C., Xia, X.,
505 and Raymond, P. A.: The importance of hydrology in routing terrestrial carbon to the atmosphere via global streams and rivers, Proceedings of the National Academy of Sciences, 119, e2106322119, doi:10.1073/pnas.2106322119, 2022.

Lorke, A., Bodmer, P., Noss, C., Alshboul, Z., Koschorreck, M., Somlai-Haase, C., Bastviken, D., Flury, S., McGinnis, D. F., Maeck, A., Mueller, D., and Premke, K.: Technical note: drifting versus anchored flux chambers for measuring greenhouse gas emissions from running
510 waters, Biogeosciences, 12, 7013-7024, 10.5194/bg-12-7013-2015, 2015.

Machado dos Santos Pinto, R., Weigelhofer, G., Diaz-Pines, E., Guerreiro Brito, A., Zechmeister-Boltenstern, S., and Hein, T.: River-floodplain restoration and hydrological effects on GHG emissions: Biogeochemical dynamics in the parafluvial zone, Science of The Total Environment, 715, 136980, https://doi.org/10.1016/j.scitotenv.2020.136980, 2020.

Maeck, A., Hofmann, H., and Lorke, A.: Pumping methane out of aquatic sediments - ebullition forcing mechansims in an impounded river, biogeosciences, 11, 2925-2938, 2014.

515 Maier, M. S., Teodoru, C. R., and Wehrli, B.: Spatio-temporal variations in lateral and atmospheric carbon fluxes from the Danube Delta, Biogeosciences, 18, 1417-1437, 10.5194/bg-18-1417-2021, 2021.

Mallast, U., Staniek, M., and Koschorreck, M.: Spatial upscaling of CO_2 emissions from exposed river sediments of the Elbe River during an extreme drought, Ecohydrology, 13, ARTN e221610.1002/eco.2216, 2020.

Marcé, R., Obrador, B., Gómez-Gener, L., Catalán, N., Koschorreck, M., Arce, M. I., Singer, G., and von Schiller, D.: Emissions from dry
520 inland waters are a blind spot in the global carbon cycle, Earth-Science Reviews, 188, 240-248, https://doi.org/10.1016/j.earscirev.2018.11.012, 2019.

Matoušů, A., Rulík, M., Tušer, M., Bednařík, A., Šimek, K., and Bussmann, I.: Methane dynamics in a large river: a case study of the Elbe River, Aquat Sci, 81, 12, 2019.

Migne, A., Gevaert, F., Creach, A., Spilmont, N., Chevalier, E., and Davoult, D.: Photosynthetic activity of intertidal microphytobenthic
525 communities during emersion: in situ measurements of chlorophyll fluorescence (PAM) and CO2 flux (IRGA), J Phycol, 43, 864-873, 10.1111/j.1529-8817.2007.00379.x, 2007.

Palmer, M., and Ruhi, A.: Measuring Earth's rivers, Science, 361, 546-547, doi:10.1126/science.aau3842, 2018.

Paranaíba, J. R., Aben, R., Barros, N., Quadra, G., Linkhorst, A., Amado, A. M., Brothers, S., Catalán, N., Condon, J., Finlayson, C. M., Grossart, H.-P., Howitt, J., Oliveira Junior, E. S., Keller, P. S., Koschorreck, M., Laas, A., Leigh, C., Marcé, R., Mendonça, R., Muniz, C.
530 C., Obrador, B., Onandia, G., Raymundo, D., Reverey, F., Roland, F., Rõõm, E.-I., Sobek, S., von Schiller, D., Wang, H., and Kosten, S.: Cross-continental importance of CH_4 emissions from dry inland-waters, Science of The Total Environment, 151925, https://doi.org/10.1016/j.scitotenv.2021.151925, 2021.

Phillips, C. L., Nickerson, N., Risk, D., and Bond, B. J.: Interpreting diel hysteresis between soil respiration and temperature, Global Change Biol, 17, 515-527, 10.1111/j.1365-2486.2010.02250.x, 2011.

535 Pusch, M., and Fischer, H.: Stoffdynamik und Habitatstruktur in der Elbe, Weißensee, Berlin, 2006.

R-Core-Team: R: A language and environment for statistical computing. R Foundation for Statistical Computing, Vienna, Austria, 2016.

Raymond, P. A., Zappa, C. J., Butman, D., Bott, T. L., Potter, J., Mulholland, P., Laursen, A. E., McDowell, W. H., and Newbold, D.: Scaling the gas transfer velocity and hydraulic geometry in streams and small rivers, Limnology and Oceanography-Fluids&Environment, 2, 41-53, 2012.

540 Raymond, P. A., Hartmann, J., Lauerwald, R., Sobek, S., McDonald, C., Hoover, M., Butman, D., Striegl, R., Mayorga, E., Humborg, C., Kortelainen, P., Durr, H., Meybeck, M., Ciais, P., and Guth, P.: Global carbon dioxide emissions from inland waters, Nature, 503, 355-359, Doi 10.1038/Nature12760, 2013.

Rosentreter, J. A., Borges, A. V., Deemer, B. R., Holgerson, M. A., Liu, S., Song, C., Melack, J., Raymond, P. A., Duarte, C. M., Allen, G. H., Olefeldt, D., Poulter, B., Battin, T. I., and Eyre, B. D.: Half of global methane emissions come from highly variable aquatic ecosystem
545 sources, Nature Geoscience, 14, 225-230, 10.1038/s41561-021-00715-2, 2021.

Sander, R.: Compilation of Henry's law constants (version 4.0) for water as solvent, Atmos. Chem. Phys., 15, 4399-4981, 10.5194/acp-15-4399-2015, 2015.

Staniek, M.: Spatial distribution of greenhouse gas concentrations along two characteristic Elbe segments, bachelor, Institute of Geoscience and Geography, MLU, Halle, 2018.

550   Stanley, E. H., Casson, N. J., Christel, S. T., Crawford, J. T., Loken, L. C., and Oliver, S. K.: The ecology of methane in streams and rivers: patterns, controls, and global significance, Ecol Monogr, 86, 146-171, 10.1890/15-1027.1, 2016.

Striegl, R. G., Dornblaser, M. M., McDonald, C. P., Rover, J. A., and Stets, E. G.: Carbon dioxide and methane emissions from the Yukon River system, Global Biogeochemical Cycles, 26, https://doi.org/10.1029/2012GB004306, 2012.

Tang, M., and Kristensen, E.: Impact of microphytobenthos and macroinfauna on temporal variation of benthic metabolism in shallow coastal
555   sediments, J Exp Mar Biol Ecol, 349, 99-112, 10.1016/j.jembe.2007.05.011, 2007.

UNESCO/IHA: GHG Measurement Guidlines for Freshwater Reservoirs, edited by: Goldenfum, J. A., UNESCO, 138 pp., 2010.

Weigold, F., and Baborowski, M.: Consequences of delayed mixing for quality assessment of river water: Example Mulde-Saale-Elbe, J Hydrol, 369, 296-304, 10.1016/j.jhydrol.2009.02.039, 2009.

Wohl, E., and Iskin, E.: Patterns of Floodplain Spatial Heterogeneity in the Southern Rockies, USA, Geophys Res Lett, 46, 5864-5870,
560   10.1029/2019gl083140, 2019.